7-13-2021

Experimental evidence that metapopulation structure can accelerate adaptive evolution

Partha Pratim Chakraborty

Louis R. Nemzer

Rees Kassen

Title

Experimental evidence that metapopulation structure can accelerate adaptive evolution

Running title

Adaptive evolution in metapopulations

Authors:

Partha Pratim Chakraborty[1], Louis R. Nemzer[2] and Rees Kassen[1]

[1.] Department of Biology, University of Ottawa, Ottawa, K1N 6N5, Ontario, Canada

[2.] Department of Chemistry and Physics, Halmos College of Arts and Sciences, Nova Southeastern University, Ft. Lauderdale, FL, USA

Abstract

Whether the spatial arrangement of a population influences adaptive evolution has been a long-standing question in population genetics. In contrast to standard population genetic models, evolutionary graph theory (EGT) predicts certain topologies amplify (increase) the probability that a beneficial mutation will spread in the population relative to a well-mixed population. Here, we test these predictions empirically by tracking the fixation dynamics of an antibiotic resistant mutant under positive selection as it spreads through networks of different topologies both *in vitro* and *in silico*. We show that star-like topologies involving bi-directional dispersal between a central hub and peripheral leaves can be amplifiers of selection relative to a well-mixed network, consistent with the predictions of EGT. We further show that the mechanism responsible for amplification is the reduced probability that a rare beneficial mutant will be lost due to drift when it encounters a new patch. Our results provide the first empirical support for the prediction of EGT that spatial structure can amplify the spread of a beneficial mutation and broadens the conditions under which this phenomenon is thought to occur. We also show the importance of considering the migration rate, which is not independently adjustable in most previous models. More generally, our work underscores the potential importance of spatial structure in governing adaptive evolution by showing how the interplay between spatial structure and evolutionary forces determine the fate of a beneficial mutation. It also points the way towards using network topology to amplify the effects of weakly favoured mutations under directed evolution in industrial applications.

Introduction

Most natural populations are spatially structured, meaning they are composed of subpopulations distributed in space and connected through dispersal pathways(*1*). How network topology – the connectivity pattern among subpopulations – impacts adaptive evolution remains controversial. Calculations based on standard population genetic models of dispersal predicted little effect of spatial structure on the fixation probability (P_{fix}), the likelihood a given mutation increases in frequency to become present in all surviving individuals(*2*, *3*). However, recent work using evolutionary graph theory (EGT), in which individuals occupy the vertices of a graph, and edges correspond to connections between neighbouring sites along which they can disperse, suggests otherwise(*4*). In particular, EGT predicts that the probability a beneficial mutation arising in one node becomes fixed across the entire metapopulation depends on how nodes are connected.

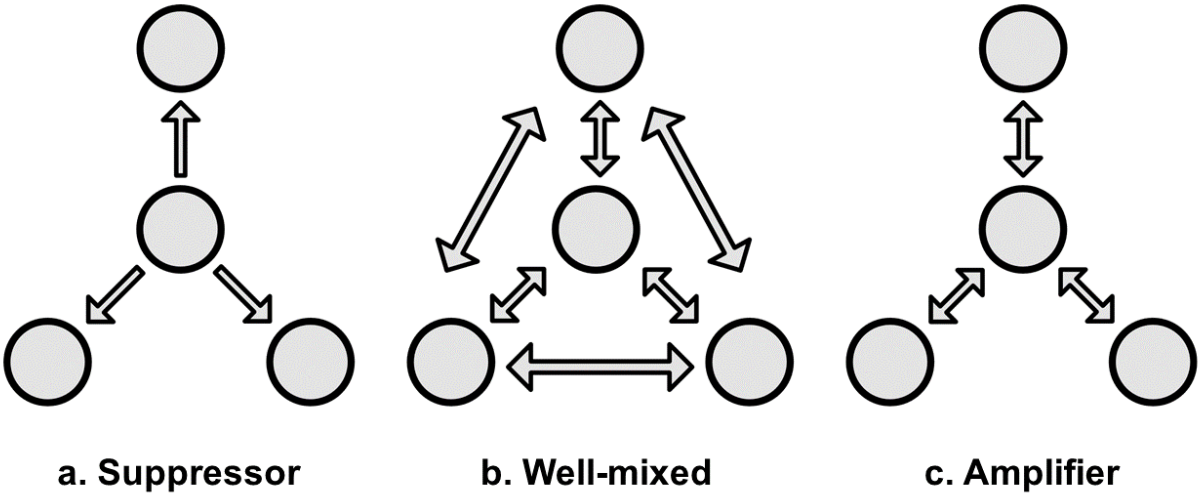

Figure 1: Three network topologies among four subpopulations. Arrows depict dispersal among subpopulations (grey circles).

To see this, consider the range of connections possible among a four-deme network (composed of satellite 'leaves' connected by a central 'hub') as illustrated in figure 1. Rooted networks (Fig 1, left panel), in which one patch supplies more individuals to others than it receives, can decrease (suppress) fixation probabilities relative to a well-mixed system (Fig 1, middle panel), because a beneficial mutant is most likely to spread through the entire network only if it arises in the hub. By contrast, networks with connections clustered in a few vertices like a star (Fig 1, right panel), can be shown to increase (amplify) fixation probabilities by as much as two-fold over a well-mixed system(*5*), because beneficial mutations arising in a leaf can spread to all other patches via the central hub.

The EGT approach has inspired a rich theoretical literature devoted to exploring the potential for ever more complicated network structures to serve as amplifiers of selection(*6*). While the original, much cited (*4*), claim that certain topologies, most notably the so-called "superstars," could asymptotically amplify even very small fitness differences, later work(*7*) has shown that this is very sensitive to the particulars of the model, such as the ordering of birth and death. Also, the standard model does not decouple reproduction and migration rates, and theoretically perfect amplification requires both unlimited space and time (*6*), raising doubts about its applicability to the real world. The fact that EGT rests on a stochastic model of evolution in finite populations (*8*) where individuals occupy the nodes of the graph means, moreover, that we do not know how robust its predictions are to more realistic situations involving nodes composed of subpopulations or variable rates of dispersal. While recent work relaxes some of the more restrictive assumptions of EGT (*9*) to show that migration asymmetry (*10*) can better account for amplification when migration is sufficiently rare to allow each node to be composed of either all wild-type or all mutant allele, the relevance of this work to real-world situations remains speculative.

A comparable effort devoted to grounding the predictions of EGT in data from real biological populations has not, to our knowledge, been undertaken. Previous experimental work on the impact of spatial structure on adaptive evolution has focused more on the role of population subdivision in governing the

magnitude or extent of adaptive change, rather than the rate or probability of fixation(*11–13*). Direct, experimental tests of the role of network topology on the rate of adaptation are lacking. Here, we use evolution experiments and agent-based simulations to investigate the impact of network topology on the fixation dynamics of a beneficial mutation.

Our experimental work tracks the spread of an initially rare beneficial mutant of *Pseudomonas aeruginosa* strain 14 (PA14) invading four-patch metapopulations varying in topology and dispersal rate. The mutant is isogenic to the wild-type save for a single base pair mutation in *gyrA* (cip^R; T83I) that confers resistance to the commonly used fluoroquinolone antibiotic ciprofloxacin and the absence of a neutral point mutation in the *lacZ* gene used to distinguish the two strains on indicator agar (see Methods). Selection is uniform across all patches and imposed by supplementing the growth media with subinhibitory concentrations of ciprofloxacin adjusted to provide a ~20% fitness advantage to the resistant type. We check our experimental results with a new agent-based simulation termed the Stochastic Agent-Based Network-Fixation Computed Topology with Undirected Migration (SANCTUM) model, in which an individual bacterium is represented by an agent that competes for finite spaces in a node, and can disperse along edges. Together, our results allow us to test directly, both *in vitro* and *in silico*, whether and how network topology modulates the fixation process that drives adaptive evolution.

The leading prediction from EGT is that bidirectional dispersal between leaf and hub patches in a star network (Fig 1c) can result in higher fixation probabilities for a beneficial mutant compared with a completely well-mixed scenario (Fig 1b). We tested this prediction experimentally by inoculating the cip^R mutant at an initial frequency of 0.001 in one leaf subpopulation and propagating the entire metapopulation under the appropriate network topology across a range of migration rates. Dispersal occurred at the time of serial transfer by first mixing samples from the appropriate subpopulations (all sub-populations in the case of a well-mixed metapopulation, bidirectional dispersal between the leaves and the central hub in the case of the star metapopulation. See supplementary information for details) and

then diluting the mixture to adjust dispersal rates. We accounted for asymmetries in the direction of migration between leaves and hub generated by bidirectional dispersal by reducing inward migration rates from the leaves to the hub by ⅓ (Fig S3). Daily transfers involved 100-fold dilutions, resulting in a bottleneck population size of ~10^7 CFUs and a maximum population size of ~10^9 CFUs, corresponding to ~6.67 generations per day. Since the theory makes predictions about fixation of a single beneficial mutation, we focus on the first 5 to 6 days (~35 to ~40 generations) to minimize the opportunity for *de novo* mutations rising to high frequency.

Results:

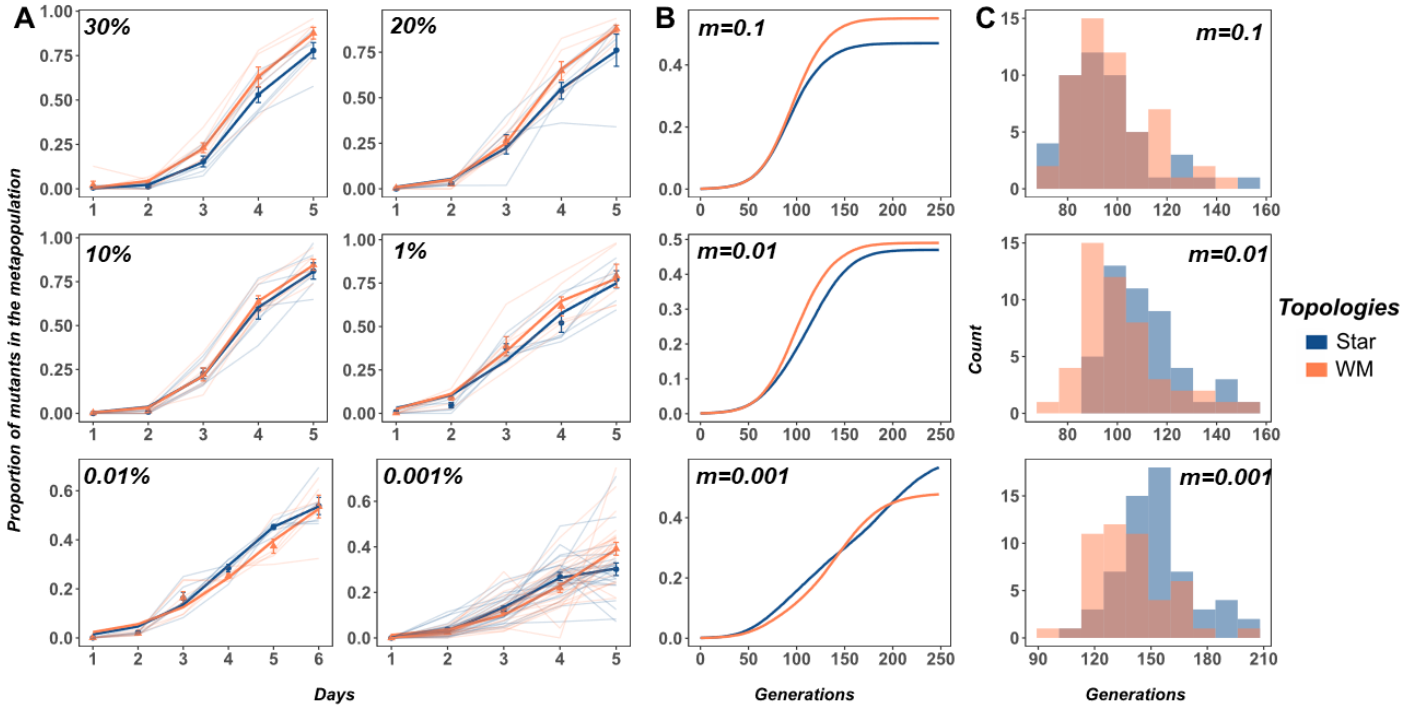

Figure 2: The proportion of cip^R mutant in replicate metapopulations (grey lines) propagated by either star (blue) or well-mixed (red) networks with unweighted migration. The bright lines depict the nonlinear least squares (NLS) fit for each metapopulation structure. Panel A shows experimental results; simulation results are shown in Panel B. Migration rates are noted in the inset of each plot. Panel C are histograms

from the simulations showing the minimum generations required for the cip^R to reach a frequency of at least 50% in a metapopulation under each combination of network type and migration rate.

Our results, shown in figure 2, are striking. Above migration rates of 1%, network topology has no noticeable effect on the spread of the cip^R mutant strain through the metapopulation. At migration rates of 0.01% and lower, however, we see a clear effect of network topology, with cip^R spreading faster in a star network than in a well-mixed system. This is consistent with the prediction from EGT that bidirectional star networks can amplify selection. Notably, the amplification effect is transient, being maximal at intermediate time steps (0.01%: relative frequency of cip^R to wt on Day 5: χ^2 =13.825, p = 0.0002 and 0.001%: frequency of cip^R on Day 4: χ^2 = 5.2577, p = 0.02185) and disappearing by the end of the experiment at days 5 or 6, depending on the migration rate (see supplementary information). This result has not been previously observed in models of EGT. While it is conceivable that amplification could be due to *de novo* evolution of second-site beneficial mutations in the cip^R background, we only observed novel colony morphotypes in the more abundant wild-type background. When present, these had undulate morphologies indicative of biofilm formation. Our observation that amplification occurred in spite of potential competition from *de novo* mutants makes our results even more compelling.

To confirm these results are not an idiosyncratic feature of our biological system, and to provide additional insight into the mechanisms driving amplification, we modelled the population dynamics of selection in metapopulations under the same topologies and migration rates using the agent-based SANCTUM model. Nodes each contained a fixed number of spaces, here 1600, which can independently be empty, occupied by a wild-type bacterium, or occupied by a mutant. In contrast with simpler models that allow each node to have exactly two states - either all wild type or all mutant - the SANCTUM model is a much more realistic representation of natural systems, including our experiment, in that it can accomodate populations of various sizes and mutant fraction in each node. Dispersal occurs between nodes connected by edges, and the fitness is given by the probability of being killed by the antibiotic,

which depends on whether or not the genotype is resistant to it. Our model thus allows us to properly capture the dynamics of slow, but nonequilibrium, migration. The results of our simulations are shown in Fig 2B-C and match our experimental results very closely, with little noticeable effect of topology at high migration rates and transient amplification under low migration rates.

Closer inspection of the simulation results suggests that amplification is most likely to occur when the expected number of mutant migrants per generation at the effective carrying capacity is on the order of one, that is:

$$Expected\ Migrants\ per\ Step\ =\ (Migration\ Rate)\ x\ (Spaces\ per\ Node)\ x\ [1\ -\ (Antibiotic/Resistance)]\ \sim\ 1.$$

This result suggests that amplification associated with "slow" migration rates is caused by seeding events of mutants into a new node if and only if the mutants have already successfully colonized a previous node. The substitution process therefore occurs in a more predictable and stepwise fashion under slow migration, compared with fast migration rates, because beneficial mutants are less likely to be lost due to drift when they colonize an empty node.

Our experiments adjust the migration rate, m, to ensure all patches receive the same number of mutants. Recent theoretical work, which considers nodes as subpopulations rather than individuals as in our experiments, shows that asymmetry in migration between leaves and the hub in star networks can potentially amplify probabilities of fixation relative to the well-mixed case. Specifically, star networks with net outward or inward migration have been predicted to be suppressors or amplifiers of selection, respectively, while those with no net inward or outward, or balanced, migration have been shown to have no advantage over a well-mixed network in fixing a beneficial mutant(*9*). Our experimental set-up and modelling framework allow us to test these predictions by manipulating the relative amount of migration between the hub and the three leaves of the star network.

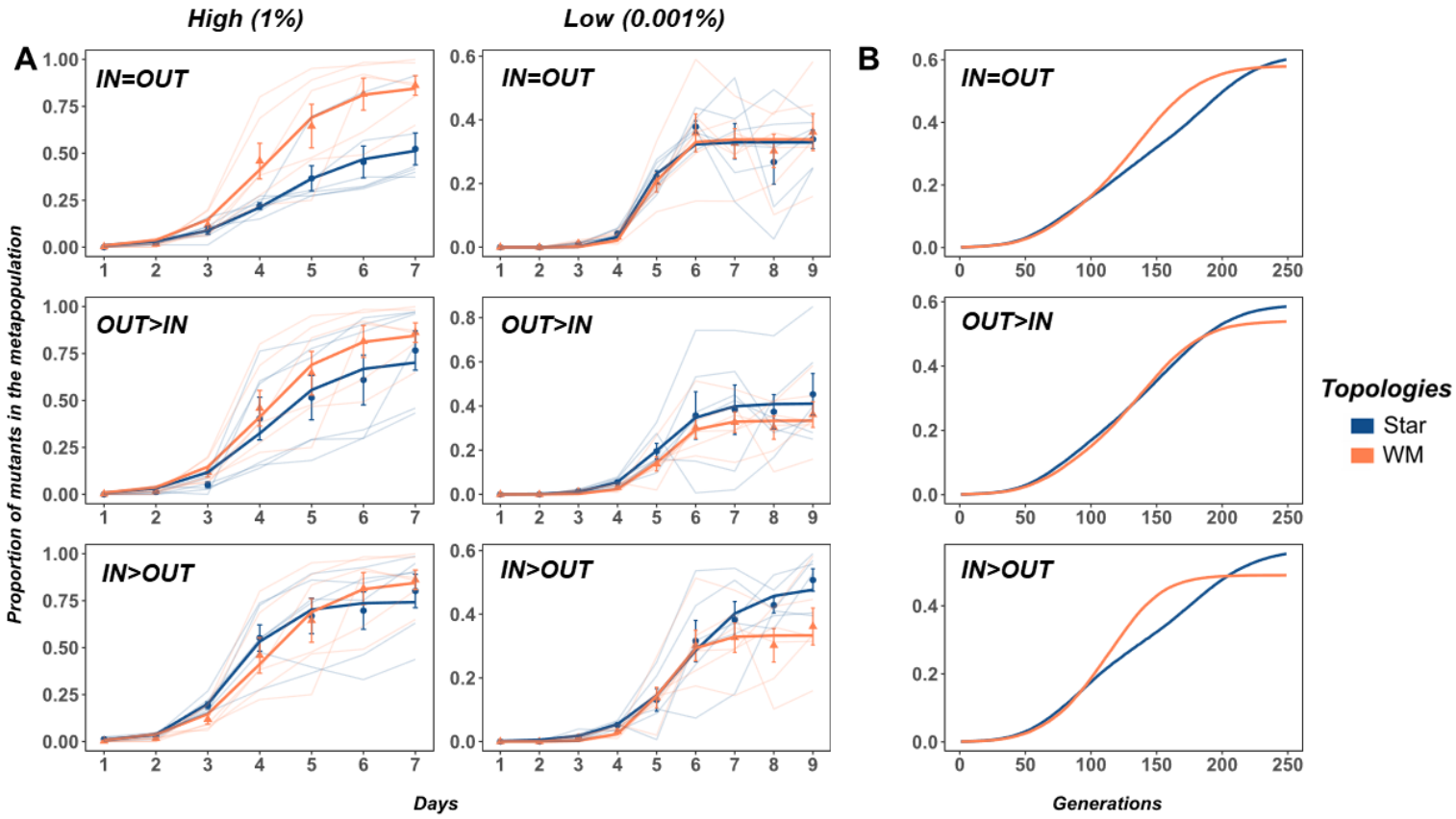

Figure 3: The proportion of cip^R mutant in replicate metapopulations (grey lines) propagated on either star (blue) or well-mixed (red) networks with weighted migration. Bright lines are the nonlinear least squares (NLS) fit to the two network treatments. Panel A shows results from the experiments under high and low migration rates, whereas Panel B shows the results of the SANCTUM model only under the low migration rate. The respective dispersal asymmetries are provided in the inset of each plot.

Our results are consistent with the predictions of theory. At high migration rates (Fig 3A), the rate at which the cip^R mutant spreads in a star network never exceeds (see supplementary information) that of the well-mixed topology under both forms of asymmetric migration (middle and bottom panels), and is substantially slower when migration rates were balanced among the nodes (top panel) (IN=OUT: relative

frequency of cip^R on Day 9: $\chi^2 = 12.234$, p = 0.00047) . A different picture emerges at low migration rates (Fig 3B). Now, the dynamics of cip^R spread in star networks is indistinguishable (see supplementary information) from that of the well-mixed case for both balanced migration (top panel) and net outward migration (middle panel), as expected from theory. However, this is not the case when inward migration exceeds outward migration (bottom panel), where the cip^R mutants gain a significant advantage in the latter stages of the experiment (IN>OUT: relative frequency of cip^R on Day 9: $\chi^2 = 5.2917$, p = 0.02143). The results of our simulations are shown in the panels in Fig 3C and match our experimental results very closely.

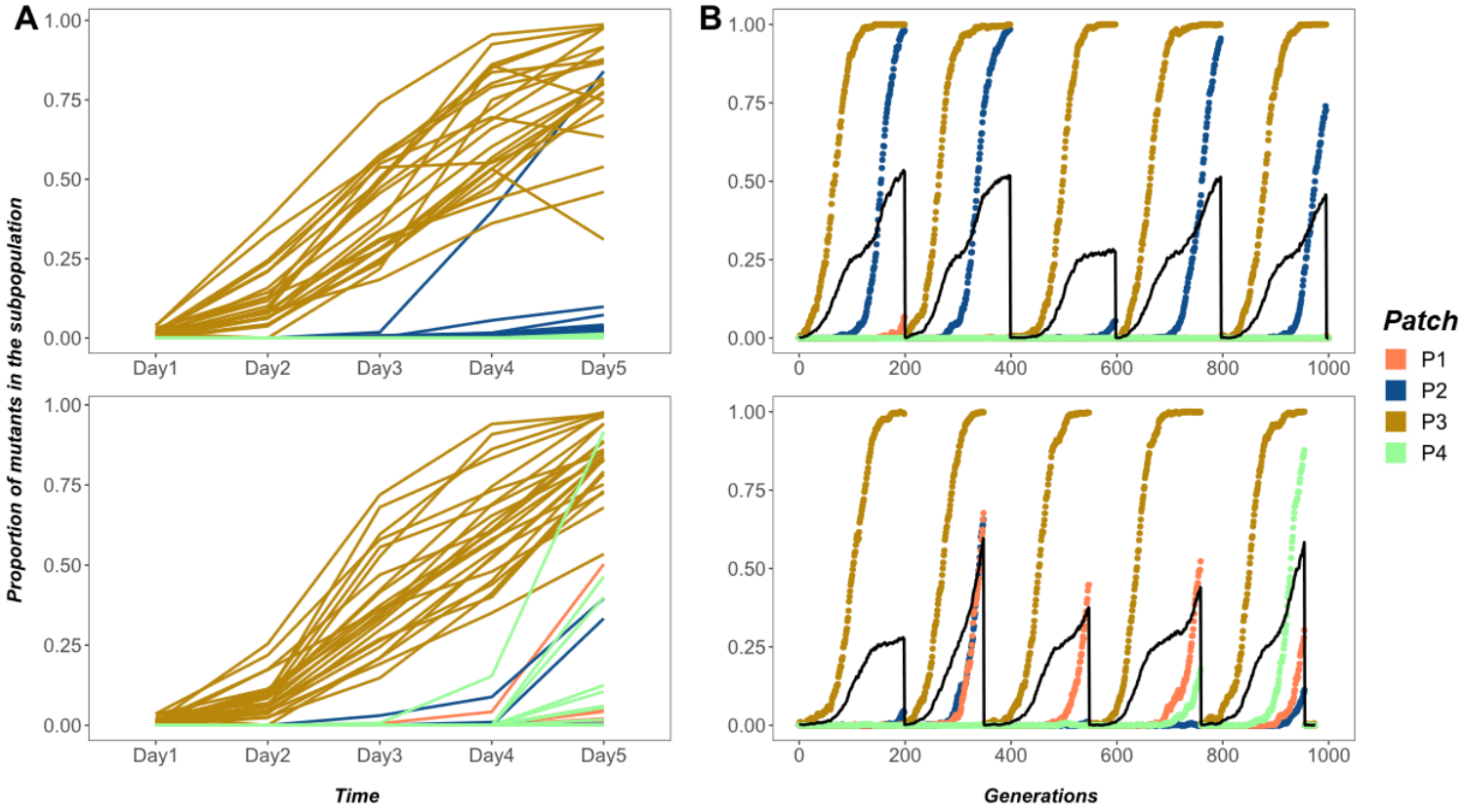

Figure 4: The proportion of the cip^R mutants in the constituent subpopulations of each replicate metapopulation propagated as either star (both panel A and B, first row) or well-mixed (both panel A and B, second row) networks with unweighted migration of 0.001% (~100 individuals). Panel A is the data from the experiment and Panel B is the data from the SANCTUM model. Subpopulation nomenclature:

P3 = node of introduction of the cip^R mutant, P2 = hub and P1 and P4 = rest of the peripheral leaves. In panel A, cip^R fixation dynamics in four subpopulations of each of the 24 replicate metapopulations under each network are shown (top = star, bottom = well-mixed). The black solid lines in panel B are the overall proportion of cip^R mutants in a metapopulation. In panel B, five replicate instantiations (each run for 200 generations) of the simulation are shown for each network (top = star, bottom = well-mixed).

The mechanism governing whether or not amplification occurs should depend on the balance between two dynamic processes, the rate of fixation in a given patch and the rate of dispersal to new patches. When migration rates are fast, an initially rare beneficial mutant cannot reach sufficiently high frequency in its native patch to guarantee dispersal to other patches. Consequently, if it does manage to get dispersed to a novel patch, the beneficial mutant is initially so rare that it is likely to be lost due to drift. Under slow migration, however, selection increases the frequency of a beneficial mutant faster in its native patch than it is dispersed to novel patches, ensuring that it can be repeatedly dispersed to novel patches and so reducing the likelihood of drift loss upon arrival. Amplifying topologies act in a similar way when dispersal is slow, by allowing beneficial mutants to first fix in the leaf in which they were introduced, and then funnelling them through a central hub, so the likelihood of drift loss before other leaves are seeded is reduced. Under well-mixed conditions, the constant influx of migrants from other patches means the beneficial mutant cannot accumulate to sufficiently high frequency in its focal patch before it is dispersed to other patches, where it is rare and likely to be lost due to drift.

We evaluated this interpretation experimentally by examining the dynamics of the cip^R mutant as it spreads among subpopulations in our experiment. Fixation should occur first in the leaf in which the beneficial mutant was initially inoculated. This is followed by, in an amplifying network, accumulation in the hub and then spread to other leaves of the network. In a well-mixed metapopulation, however, the spread of the cip^R mutant should occur more sporadically into all subpopulations, both hub and leaves, at the same time. Indeed, when we examine the dynamics of the cip^R mutant in amplifying and well-mixed metapopulations at a low migration rate (0.001%), we see the expected patterns (Fig 4). The cip^R mutant

first fixes in the leaf where it was initially inoculated for both of the networks, as expected for strong selection in a low migration regime. Although there is substantial variation among replicates, our results show that the cip^R mutant subsequently spreads quite differently among the remaining three subpopulations in the two kinds of network. Our data shows that in the amplifier network there is a clear tendency for the mutant to spread from the initial subpopulation to the hub (P2) first, whereas in the well-mixed network the mutant is equally likely to spread to the hub as any additional subpopulation (Fig 4A). These experimental results are mirrored closely by those of the simulation (Fig 4B) where the dynamics of spread in the amplifier network involve first fixation in the node of introduction, then the hub, then additional leaves.

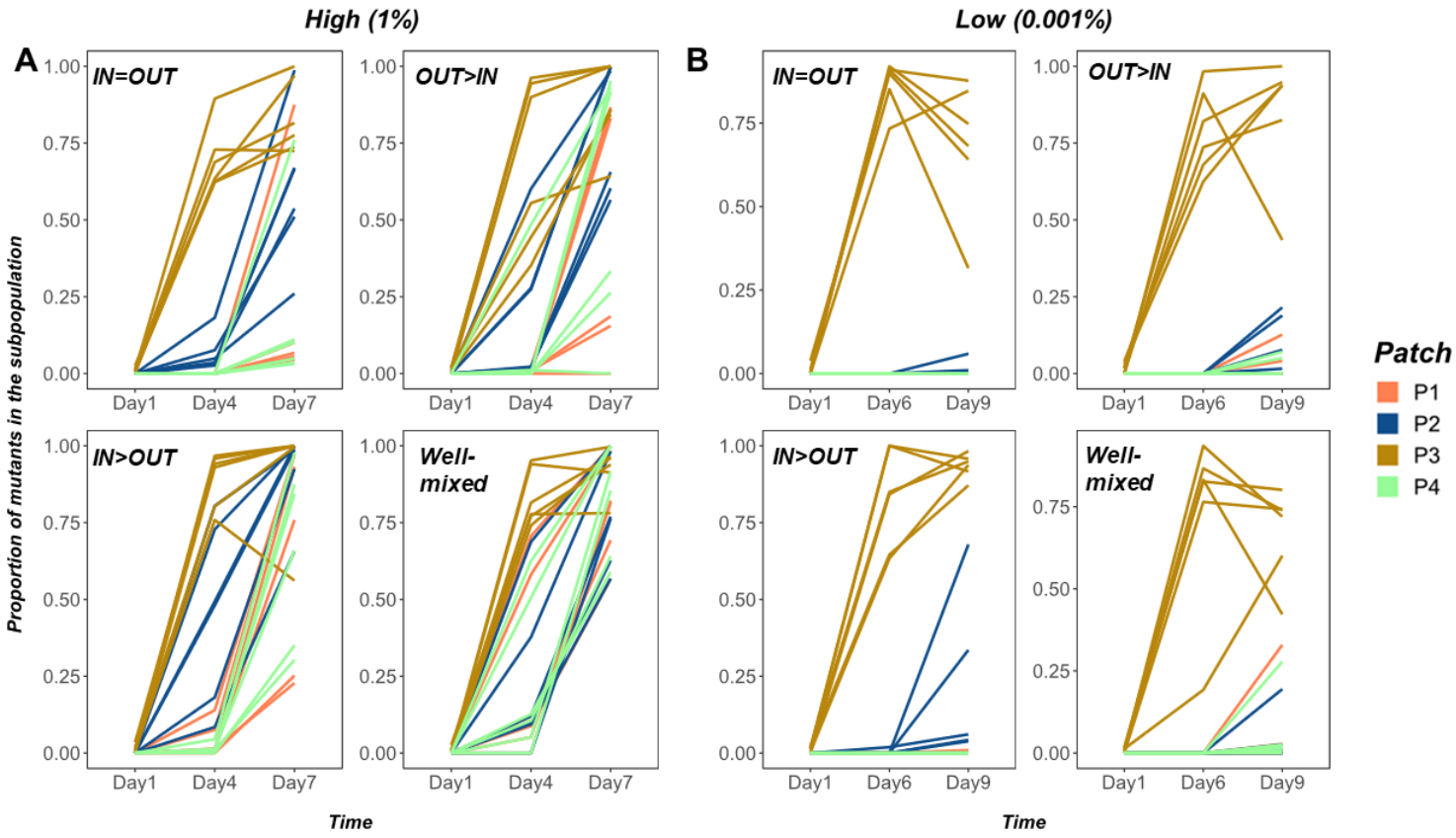

Figure 5: The proportion of the cip^R mutants in the constituent subpopulations of each metapopulation propagated by either asymmetric star or well-mixed networks under high (panel A: 1% or 10^5 individuals) and low (panel B: 0.001% or 10^2 individuals) weighted migration. Subpopulation nomenclature: P3 =

node of introduction of the cip^R mutant, P2 = hub and P1 and P4 = rest of the peripheral leaves. In both panels A and B, cip^R fixation dynamics in four subpopulations of each of the six replicate metapopulations using each of the three asymmetric star networks and the well-mixed network are shown (see plot insets for details) under high and low migration rates, respectively.

By contrast, the spread of the mutants among additional subpopulations following fixation in the node of introduction was more variable in the well-mixed population, the particular path taken being different with each run of the simulation. This dynamic of fixation in the node of introduction followed by spread to the hub and then subsequent nodes is also seen in the most strongly amplifying networks experiencing asymmetric migration (low migration rate, inward migration > outward migration; Fig 5B). Notably, the pattern of mutant spread among networks showing no evidence of amplification mirrored that seen in the well-mixed case, with the cip^R mutant spreading readily from the node of introduction to any of the other leaves (Fig 5A).

Discussion

We have shown, experimentally and through simulation, that population structure can impact the dynamics of adaptive substitution. Specifically, star metapopulations, where leaf subpopulations exchange migrants through a central hub, can act as amplifiers of selection, leading to faster rates of spread than a comparable well-mixed population where all subpopulations share migrants equally. Importantly, amplification is most pronounced when selection is strong relative to migration, a scenario that reduces the probability a rare beneficial mutant in a new patch will be lost due to drift, and when the topology of dispersal concentrates the beneficial mutant in a central hub, as in the case of asymmetric 'inward' migration. In other words, amplification occurs because rare mutants are less likely to be lost, not because the strength of selection itself increases.

This result is remarkable because it was not anticipated by standard theory in population genetics, in which population structure has been thought to have little effect on the probability of fixation for

beneficial mutants. This conclusion likely derives from the tradition in population genetics of studying allele frequency changes in infinite populations and high migration rates. In contrast, our results are consistent with - and the first experimental tests inspired by - predictions from evolutionary graph theory that identified the potential for network structure, and the star network in particular, to serve as amplifiers of selection. EGT is predicated on a model of population dynamics that focuses on finite populations by assigning individuals to the nodes of a graph. Importantly, our results show that amplification can occur under a broader and, arguably, more realistic set of conditions where populations, not individuals, occupy the nodes of a graph. Our work emphasizes the previously overlooked importance of migration rate, and serves as a first step towards bridging these two approaches, with infinite populations on the one hand and finite populations focused on the dynamics of individuals on the other.

More generally, it will be useful to expand the analytical framework of EGT to include more biological realism and to articulate more precisely the range of conditions under which amplification can occur. It should be possible, for example, to use network topology to amplify the selection of even a slightly favored mutation for the purpose of experimentation or the directed evolution of desired traits in industrial applications. A more comprehensive theory of evolution on structured landscapes will also be important in other aspects of biology, including the spread of invasive species, pathogens, and the resistance factors they possess.

Reference:

1. I. Hanski, Metapopulation dynamics. *Nature*. **396**, 41–49 (1998).
2. T. Maruyama, On the fixation probability of mutant genes in a subdivided population*. *Genetics Research*. **15**, 221–225 (1970).
3. M. Slatkin, Fixation Probabilities and Fixation Times in a Subdivided Population. *Evolution*. **35**, 477–488 (1981).
4. E. Lieberman, C. Hauert, M. A. Nowak, Evolutionary dynamics on graphs. *Nature*. **433**, 312 (2005).
5. A. Pavlogiannis, J. Tkadlec, K. Chatterjee, M. A. Nowak, Construction of arbitrarily strong amplifiers of natural selection using evolutionary graph theory. *Communications Biology*. **1**, 71 (2018).
6. J. Tkadlec, A. Pavlogiannis, K. Chatterjee, M. A. Nowak, Fast and strong amplifiers of natural selection. *Nat Commun*. **12**, 4009 (2021).
7. A. Jamieson-Lane, C. Hauert, Fixation probabilities on superstars, revisited and revised. *Journal of Theoretical Biology*. **382**, 44–56 (2015).
8. P. A. P. (Patrick A. P. Moran, *The statistical processes of evolutionary theory.* (Clarendon Press, Oxford, 1962).
9. L. Marrec, I. Lamberti, A.-F. Bitbol, *bioRxiv*, in press, doi:10.1101/2020.12.12.422518.
10. B. Adlam, K. Chatterjee, M. A. Nowak, Amplifiers of selection. *Proc. R. Soc. A*. **471**, 20150114 (2015).
11. Perfeito Lilia, Pereira M. Inês, Campos Paulo R.A, Gordo Isabel, The effect of spatial structure on adaptation in Escherichia coli. *Biology Letters*. **4**, 57–59 (2008).
12. M. Baym, T. D. Lieberman, E. D. Kelsic, R. Chait, R. Gross, I. Yelin, R. Kishony, Spatiotemporal microbial evolution on antibiotic landscapes. *Science*. **353**, 1147–1151 (2016).
13. M. G. J. L. Habets, D. E. Rozen, R. F. Hoekstra, J. A. G. M. de Visser, The effect of population structure on the adaptive radiation of microbial populations evolving in spatially structured environments. *Ecology Letters*. **9**, 1041–1048 (2006).
14. R Core Team, *R: A Language and Environment for Statistical Computing* (R Foundation for Statistical Computing, Vienna, Austria, 2020; https://www.R-project.org/).
15. J. C. Nash, *nlmrt: Functions for Nonlinear Least Squares Solutions* (2016; https://CRAN.R-project.org/package=nlmrt).
16. W. N. Venables, B. D. Ripley, *Modern Applied Statistics with S* (Springer, New York, Fourth., 2002; http://www.stats.ox.ac.uk/pub/MASS4/).
17. R. V. Lenth, *emmeans: Estimated Marginal Means, aka Least-Squares Means* (2020; https://CRAN.R-project.org/package=emmeans).

Conflicts of interest:

The authors declare no conflict of interest.

Acknowledgement:

We thank Caroline Des Ligneris for her help around the lab.

Supplementary Material:

The SANCTUM model:

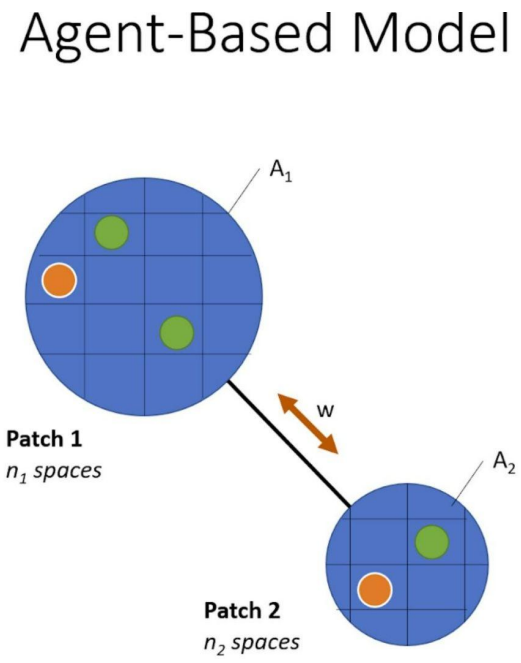

Figure S1: Schematic description of the algorithm used in the SANCTUM model.

Each patch (A_i) has n_i spaces that can each be empty, occupied by a wild-type, or occupied by a mutant. For these experiments, all the n values are set to 1600. For each generation of the simulation, there are three phases: (1) Death, (2) Birth, and (3) Migration. **Death:** An agent is removed during the death step with a probability that depends on the antibiotic concentration divided by its individual resistance. **Birth:** Each agent has a chance of reproducing an identical agent in an empty patch of the same node during the birth step. Similar to the Lotka-Volterra model of population growth, the probability of reproduction increases with the number of empty spaces in the node. **Migration:** There is a probability of migration that varies based on the experimental condition. If an agent is selected to migrate, it randomly moves to an adjacent connected node with a probability proportional to the weighting of that edge (w). The initial system is randomly seeded with one thousand agents across all nodes, and one of these is selected to be

the mutant (not in the hub). For each simulated condition, the metapopulation fraction is averaged over 100 instantiations. For runs that ultimately fix, the number of generations until the mutants are the majority of agents is also recorded.

Materials and methods

Microbial strains and conditions:

For all experiments, clonal populations of *Pseudomonas aeruginosa* strain 14:*gyrA* (PA14:*gyrA*) and PA14:*lacZ*, isogenic to PA14 except with a point mutation in the *gyrA* gene and an insertion in the *lacZ* gene respectively, were used. Colonies possessing the lacZ insertion appear blue when cultured on agar plates supplemented with 40 mg/L of 5-bromo-4-chloro-3-indolyl-beta-D-galactopyranoside (X-Gal), and are visually distinct from the PA14:*gyrA* white colouration. The neutrality of the *lacZ* marker was confirmed in our experimental environments by measuring the fitness of the marked strain relative to the unmarked strain (Figure S5). Populations were cultured in 24-well plates with 1.5 mL of media in each well, in an orbital shaker (150 RPM) at 37°C. The culture media consisted of Luria Bertani broth (LB: bacto-tryptone 10 g/L, yeast extract 5 g/L, NaCl 10 g/L) supplemented with 20 ng/mL of the fluoroquinolone antibiotic, ciprofloxacin. This concentration of ciprofloxacin confers ~ 20% selective advantage to PA14:*gyrA* relative to PA14:*lacZ* (inferred from antibiotic concentration window shown in S5). All strains and evolving populations were frozen at −80°C in 20% (v/v) glycerol.

Evolution experiment:

A single metapopulation consisted of four subpopulations, one subpopulation being located on each of four different 24-well plates. Plate 2 was always assigned as the hub, and plates 1, 3, and 4 were treated as the leaves. This design allows us to track up to 24 replicate populations using just four multi-well plates. The experiment was initiated by inoculating each subpopulation with ~10^7 colony forming units (CFU) per ml of PA14:*lacZ* descended from a single colony picked from an agar plate and grown overnight in

liquid LB at 37°C with vigorous shaking (150 RPM). The cip^R mutant, derived from frozen cultures in the same way, was introduced simultaneously into one subpopulation (plate 3) at a density ~10^4 PA14:*gyrA* cells producing an initial ratio of resistant to wild-type cells of ~1:1000 in this subpopulation. Metapopulations were transferred daily following dispersal among subpopulations (see below) by taking an aliquot corresponding to ~10^7 CFUs per mL and inoculating into fresh medium. The population density in each subpopulation reached ~10^9 CFUs, so this transfer regime corresponds to ~6.67 daily generations of growth.

We constructed distinct network topologies by mixing subpopulations prior to serial transfer following the schematic shown in Fig S2. Briefly, well-mixed networks were created by combining equal volume aliquots from all subpopulations into a common dispersal pool, diluting this mixture to the appropriate density to achieve the desired migration rate, and then mixing the dispersal pool with aliquots from each subpopulation (so-called 'self-inoculation') before transfer. Star networks, which involve bidirectional dispersal between the hub and leaves, were constructed in a similar way to the well-mixed situation only now the dispersal pool consisted of aliquots from just the leaves and aliquots from the hub (plate 2) were mixed with 'self-inoculation' samples from each leaf prior to serial transfer. Further details on how each network topology and migration rate were achieved are provided in Appendix 1.

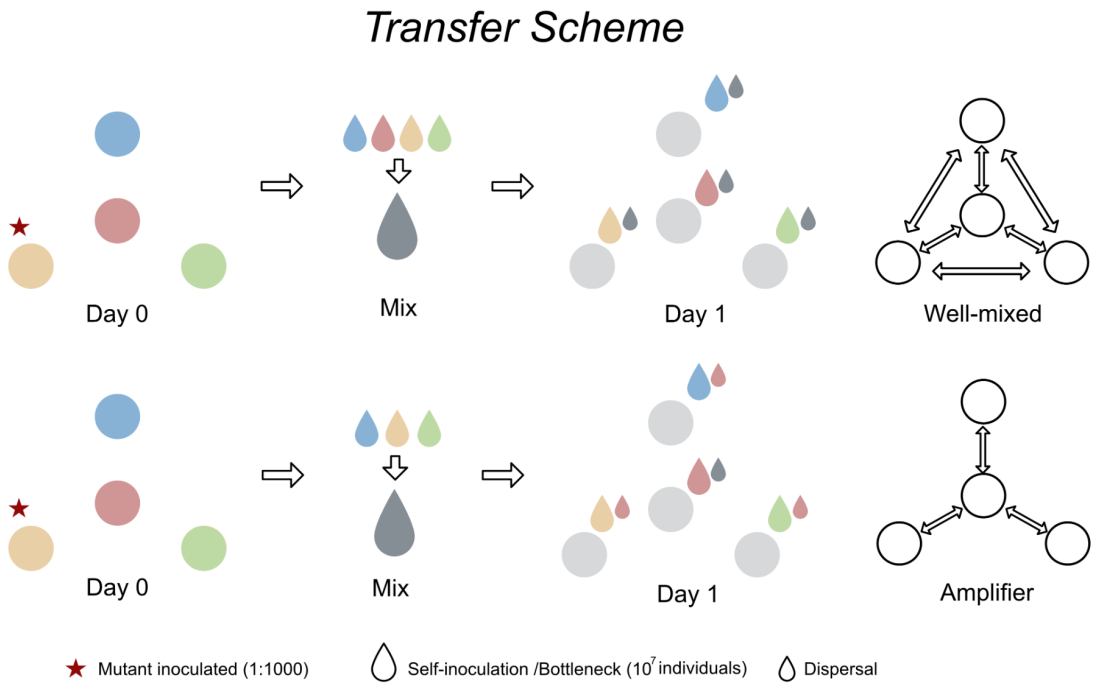

Figure S2: Transfer scheme to experimentally create star and well-mixed network structures.

Tracking the spread of resistance:

We tracked the spread of the cip^R mutant (PA14:*gyrA*) relative to the wild type (PA14:*lacZ*) by plating samples from each subpopulation as well as a mixture of the entire metapopulation on LB agar plates supplemented with X-gal allowing us to use blue-white screening to track the relative frequency of each type over time.

Statistical analyses:

All statistical analyses were conducted using the R statistical software(*14*). We used two complementary approaches to analyse our experimental data.

The first models the spread of resistance (see Fig. 2 and Fig. 3) as a three-parameter logistic growth model using non-linear least squares with a fixed N0 (NLS) (*15*). This model, as with comparable approaches focused on population growth in resource limited environments, allows us to estimate the rate

at which resistance spreads (equivalent to r_{max} in logistic growth) and the final frequency of cip^R mutants at the end of the experiment (equivalent to the carrying capacity, K, from logistic growth models) in each replicate metapopulation. Contrasts of maximal growth rates between treatments (star or well-mixed) were performed using a linear model (lm function from base R). Comparable contrasts for maximum proportion of resistant mutants fixed on the final day of the experiment used a generalized linear mixed model using methods as described below.

The second approach modelled the change in proportion for the cip^R mutants directly using a generalized linear mixed model (GLMM) with quasi-binomial error distribution (and logit link function), using the glmmPQL function from the MASS package in R(*16*). We focus on the main effects of time and network structure (star vs. well-mixed) and their interaction at each migration rate treatment. Logistical constraints prevented us from conducting experiments that manipulate both network structure and migration rate simultaneously, so we elected to run separate experiments at each migration rate to focus on the effect of contrasting network structures, as this is the focus of EGT. Our model treats 'network' as a fixed effect and 'replicate' as a random effect, while accounting for repeated measures through time. This approach produces estimates of the pairwise difference between the slopes (vs time) for the network treatment (for example, - Time:Network $_{star}$ - Time:Network $_{well\text{-}mixed}$) that were further analysed using the EMTRENDS function from the EMMEANS package (analogous to a Tukey *post hoc* test) (*17*). These contrasts allow us to examine the magnitude and direction of difference between the star and well-mixed networks for the whole experiment.

The approaches above, which focus on estimating best-fit main effects and interactions, are useful for helping to visualize the dynamics of spread across many instantiations of an inherently noisy process. We additionally focus attention on contrasts between the fraction of cip^R mutants between star and well-mixed treatment at specific days when: (1) the fitted logistic model for the star was higher than that of the well-mixed over the course of the complete experiment; or, (2) when the fitted models reveal a transient "crossover" event at intermediate time steps. We used a GLMM as described above to contrast the

fraction of cip^R mutants in star vs well-mixed networks at a particular day, treating replicate as a random factor. The analysis of variance of the GLMMs were performed with the ANOVA function from the CAR package.

```
Full_model<-glmmPQL(Proportion~Time*Treatment, random = 1|Replicate, family = quasibinomial, data)

em1<- emtrends(Full_model, pairwise ~ Treatment, var = 'Time')

em1$contrasts

model_K <- glmmPQL(Proportion ~ Treatment , random= ~1|Rep, family = quasibinomial, data)  #takes data from final day of the experiment/ change the data to get any particular day

model_R<-lm(R~Treatment, data)
```

<Appendix 1. Detailed methods used to construct network topologies.>

Unweighted migration:

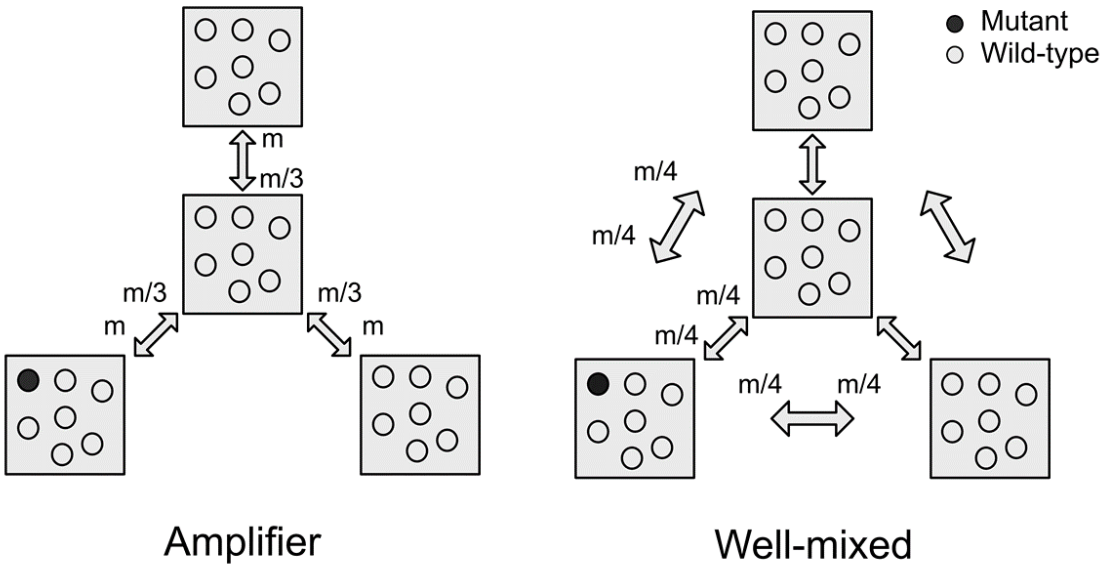

Figure S3: Schematics depicting the amount of transferred migrants per edge connection in the cases of unweighted migration regime for star and well-mixed networks.

Well-mixed: 35µL of subpopulations 1, 2, 3 and 4 were mixed together, and 20 µL from this resulting pool of migrants (MIX) was serially diluted in fresh media supplemented with 20 ng/mL Ciprofloxacin to achieve ~10^8, ~10^7, ~10^5 and ~10^4 CFU/mL. Then, 15 µL of the diluted MIX was added to 1.5 mL of fresh media along with 15 µL of the previous day's culture to achieve desired migration levels of ~10^6, ~10^5, ~10^3 and ~10^2 CFU/mL. For 20% and 30% migration, 30 µL and 45 µL of the diluted MIX were added with the culture from the previous day.

Amplifier: 35 µL of subpopulations 1, 3 and 4 were mixed together, and 20 µL from this resulting pool of migrants (MIX) was serially diluted in fresh media and 20 ng/mL antibiotic to reach ~10^8, ~10^7, ~10^5 and ~10^4 CFU/mL. On the other hand, 20 µL of subpopulation 2 (HUB) was serially diluted in fresh media and 20 ng/mL Ciprofloxacin to reach ~10^8, ~10^7, ~10^5 and ~10^4 CFU/mL. Then, 15 µL of the diluted MIX was added to 1.5 mL fresh media along with 15 µL of the previous day's subpopulation 2 culture to achieve the desired migration levels of ~10^6, ~10^5, ~10^3 and ~10^2 CFU/mL. Also, 15µL of the diluted HUB was added to 1.5 mL fresh media along with the previous day's culture to achieve desired migration levels of ~10^6, ~10^5, ~10^3 and ~10^2 CFU/mL in subpopulations 1, 3 and 4. For 20% and 30% migration, 30 µL and 45 µL of the diluted MIX were added after the bottleneck("self inoculation").

Asymmetric migration:

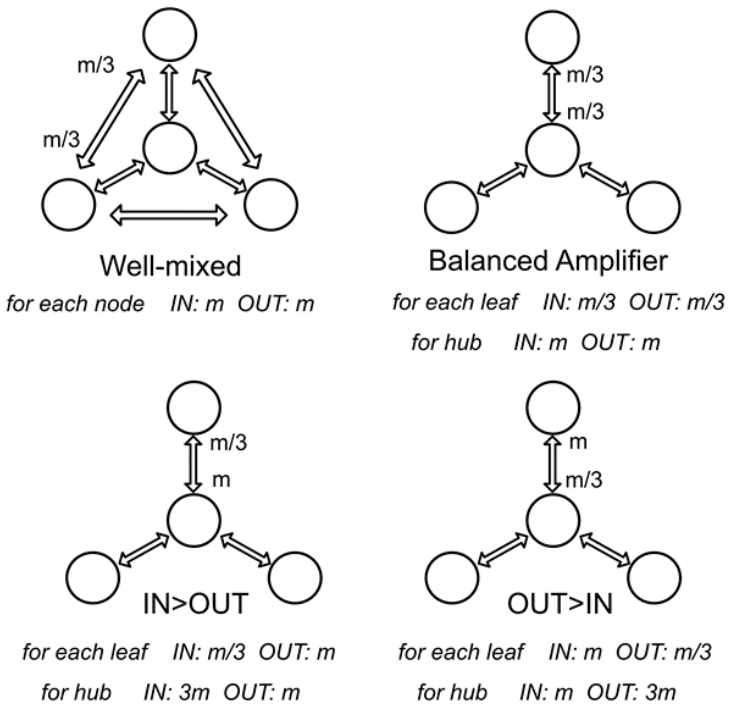

Figure S4: Schematics depicting transferred migrants per edge connection in case of the weighted migration regimes for three asymmetric star networks and the well-mixed network.

Well-Mixed: 20 µL of subpopulation 1,2,3 and 4 (MIX) were mixed in 120 µL of fresh culture media with 20 ng/mL Ciprofloxacin and serially diluted to reach ~4 x 10^7 or ~4 x 10^4 CFU/mL. Then, 15 µL of the diluted MIX was added to 1.5 mL fresh media along with 15 µL of the previous day's culture. This resulted in the transfer of 4 x 10^5 for the high migration rate experiments, or 4 x 10^2 CFU/mL for the low migration rate.

Balanced star (IN = OUT): 20 µL of subpopulations 1, 3, and 4 (MIX) were mixed in 140 µL of fresh culture media with 20 ng/mL Ciprofloxacin and serially diluted to reach ~3 x 10^7 or ~3 x 10^4 CFU/mL. Also, 20 µL of subpopulation 2 (HUB) was mixed in 180 µL of fresh culture media with 20 ng/mL Ciprofloxacin and serially diluted to reach ~10^7 or ~10^4 CFU/mL. This resulted in the transfer of ~3 x 10^5 and ~3 x 10^2 CFU/mL to the hub, and ~10^5 and ~10^2 CFU/mL to the peripheral leaves, for the high and low migration rates, respectively.

OUT>IN regime: 20 µL of subpopulation 1, 3, and 4 (MIX) were mixed in 140 µL of fresh culture media with 20 ng/mL Ciprofloxacin and serially diluted to reach ~3 x 10^7 or ~3 x 10^4 CFU/mL. Also, 60 µL of subpopulation 2 (HUB) were mixed in 140 µL in fresh culture media with 20 ng/mL Ciprofloxacin and serially diluted to reach ~3 x 10^7 or ~3 x 10^4 CFU/mL. This resulted in the transfer of ~3 x 10^5 or ~3x 10^2 CFU/mL to the hub and ~3 x 10^5 or ~3 x 10^2 CFU/mL to the peripheral leaves, for the high and low migration rates, respectively.

IN>OUT regime: 60 µL of subpopulation 1, 3, and 4 (MIX) were mixed in 20 µL of fresh culture media with 20 ng/mL Ciprofloxacin and serially diluted to reach ~9 x 10^7 or ~9 x 10^4 CFU/mL. Also, 20µL of subpopulation 2 (HUB) was mixed in 180 µL of fresh culture media with 20 ng/mL Ciprofloxacin and serially diluted to reach ~10^7 or ~10^4 CFU/mL. This resulted in the transfer of ~9 x 10^5 or ~9 x 10^2 CFU/mL to the hub and ~10^5 or ~10^2 CFU/mL to the peripheral leaves, for the high and low migration rates, respectively.

Statistical results for the full models and the nls:

Full models:

Unweighted:

Migration rate	Simple slope contrasts (Trt1 - Trt2)*time	Estimate	SE	DF	t ratio	p-value
30%	AMP - WM	-0.0212	0.156	51	-0.136	0.8923
20%	AMP - WM	-0.32	0.158	51	-2.023	0.0483
10%	AMP - WM	-0.0915	0.156	51	-0.585	0.5613
1%	AMP - WM	-0.0158	0.139	51	-0.114	0.9097
0.01%	AMP - WM	0.011	0.0834	63	0.132	0.8956
0.001%	AMP - WM	-0.198	0.0732	213	-2.708	0.0073

Weighted:

Migration rate	Simple slope contrasts (AMPx - WM)* Time	Estimate	SE	DF	t ratio	p-value
High	In = Out	-0.489	0.121	140	-4.032	0.0005
	In < Out	-0.111	0.134	140	-0.832	0.8392
	In > Out	-0.295	0.121	140	-2.432	0.0758
Low	In = Out	-0.0364	0.0743	188	-0.490	0.9612
	In < Out	0.0695	0.0766	188	0.907	0.8012
	In > Out	0.1376	0.0797	188	1.728	0.3123

NLS:

Unweighted:

Migration rate	Rate of increase (analogous to R in a logistic growth model)	Final frequency (analogous to K in a logistic growth model)	Conclusion:
30%	$F_{1,10}$ =1.623, p = 0.2315	χ^2 = 15.348, p = 8.94e-05 (EXPT 5th day) χ^2 = 8.4269, p = 0.003697 (NLS)	WM has a significantly higher K but R is not significantly different between AMP and WM
20%	$F_{1,10}$ = 0.9149, p = 0.3614	χ^2 = 9.0148, p = 0.002678 (EXPT 5th day) χ^2 = 6.5309 , p = 0.0106 (NLS)	WM has a significantly higher K but R is not significantly different between AMP and WM
10%	$F_{1,10}$ = 0.0515, p = 0.825	χ^2 = 0.7082, p = 0.4001 (EXPT 5th day) χ^2 = 0.1777, p = 0.6734 (NLS)	R and K is not significantly different between AMP and WM
1%	$F_{1,10}$ = 0.0258, p = 0.8757	χ^2 = 0.2168, p = 0.6415 (EXPT 5th day) χ^2 = 1e-04, p = 0.9908 (NLS)	R and K is not significantly different between AMP and WM
0.01%	$F_{1,10}$ = 0.1229, p = 0.7331	χ^2 = 0.0021, p = 0.963 (EXPT 6th day) χ^2 = 1.5471, p = 0.2136 (NLS)	R and K is not significantly different between AMP and WM
0.001%	$F_{1,46}$ = 1.542, p = 0.2206	χ^2 = 5.4046, p = 0.02008 (EXPT 5th day) χ^2 = 9.2005, p= 0.00242 (NLS)	WM has a significantly higher K but R is not significantly different between AMP and WM

Weighted:

Comparisons	Migration	Rate of increase (analogous to R in a logistic growth model)	Final frequency (analogous to K in a logistic growth model)	Conclusion
In = Out vs. WM	High (1%)	$F_{1,10}$ =4.8754, p = 0.05173	χ^2 = 12.234, p = 0.0004694 (EXPT 7th day) χ^2 = 13.19 , p = 0.0002815 (NLS)	WM has a significantly higher K but R is not significantly different between AMP and WM
	Low (0.001%)	$F_{1,10}$ =0.6108, p = 0.4526	χ^2 = 0.1848, p = 0.6673 (EXPT 9th day) χ^2 = 0.8844, p = 0.347 (NLS)	R and K is not significantly different between AMP and WM
Out>In vs. WM	High(1%)	$F_{1,10}$ =0.1022, p =0.7557	χ^2 = 1.1888, p = 0.2756 (EXPT 7th day) χ^2 = 0.6612, p = 0.4161 (NLS)	R and K is not significantly different between AMP and WM
	Low(0.001%)	$F_{1,10}$ =0.2279, p = 0.6434	χ^2 = 0.5233, p = 0.4694 (EXPT 9th day) χ^2 = 2.1761, p = 0.1402 (NLS)	R and K is not significantly different between AMP and WM
In>Out vs. WM	High (1%)	$F_{1,10}$ =0.7773, p = 0.3986	χ^2 = 0.4124, p = 0.5208 (EXPT 7th day) χ^2 = 1.1907, p = 0.2752 (NLS)	R and K is not significantly different between AMP and WM
	Low(0.001%)	$F_{1,10}$ =0.9051, p = 0.3638	χ^2 = 5.2917, p = 0.02143 (EXPT 9th day) χ^2 = 5.7524, p = 0.01647 (NLS)	AMP has a significantly higher K but R is not significantly different between AMP and WM

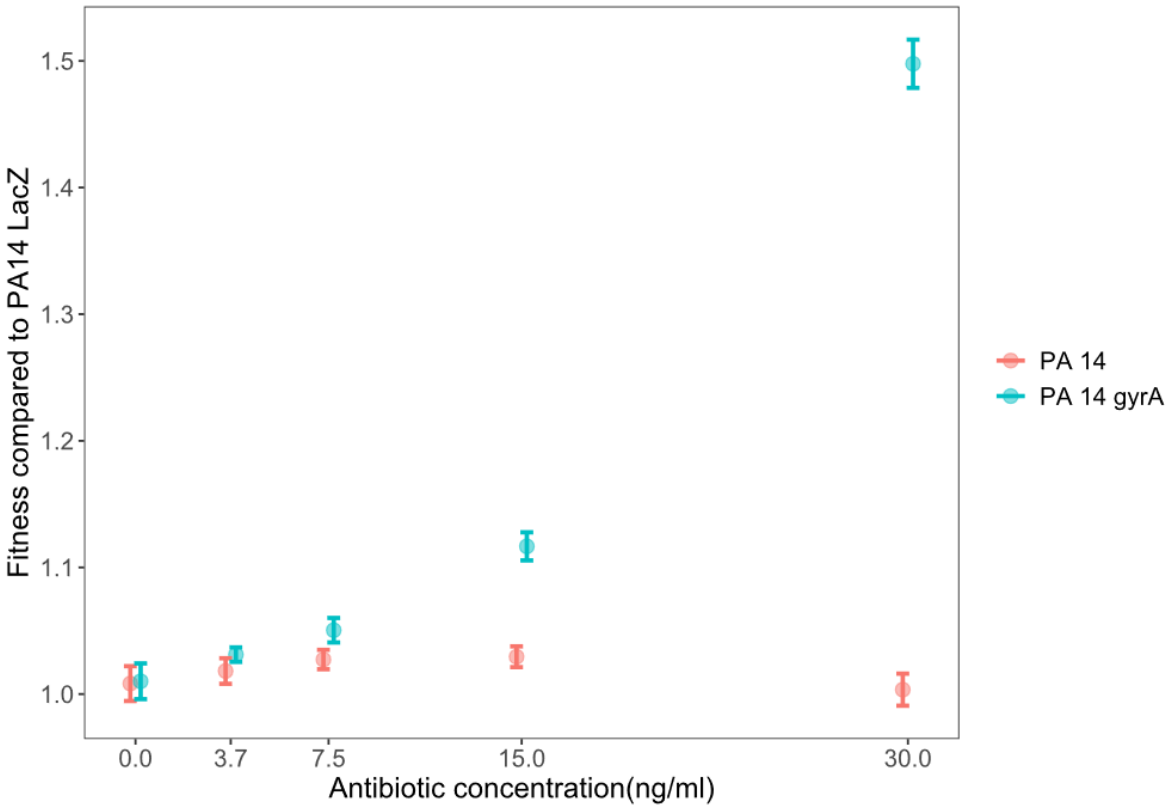

Figure S5: The fitness of PA-14 and PA14:*gyrA* competed separately against PA-14:*LacZ* under very low antibiotic (Ciprofloxacin) concentrations. PA-14:*LacZ* does not incur any cost, nor does it have any fitness advantage, over the entire range of antibiotic concentrations chosen, including the concentration used in the experiments (20 ng/mL).